

# Design and Analysis of Case to Case Segment Joint for Aerospace Applications

Samia Fida<sup>1</sup>, Asif Israr<sup>2</sup>

**Abstract** — Solid Rocket Motors (SRMs) serve as the propulsion devices for satellite-launchers. High stiffness values, high strength to weight ratios and greater mechanical/structural properties of composite materials make composite SRMs more efficient than metallic SRMs. The disadvantage of composite SRMs lies in the joining of segments. Segmented SRMs are essential when requirement is of large size and high payload. In segmentation the reliability of the whole structure depends upon the efficiency of the segment joint. Therefore the joint must be proficient enough to withstand the structural and dynamic loads. The progressive damage analysis is used to evaluate the mechanical performance of composite structure, the damage mechanism and its progression. Internal combustion of exhaust gases creates hoop stresses inside the SRMs case. These hoop stresses induce the bending moments in the joint section of segmented SRMs. In this study the various segment joint parameters are analyzed i.e. number of pins, pin material and pin diameter. The effect of each parameter on joint strength of SRM is evaluated to conclude the optimum joint parameters. After the selection of optimum joint parameters, the progressive damage analysis is carried out to analyze the behavior of composite segment joint against the proposed operating conditions. The proposed joint design is analyzed at different operating pressures to find out the critical failure mechanism of composite SRM.

**Keywords**—Solid Rocket Motors (SRMs); Stiffness; Propulsion; Fiber reinforced composite; Segmented; Joints; Progressive Damage Analysis

## I. INTRODUCTION

Solid Rocket Motors (SRMs) are classified as non-air breathing propulsion system. The design and manufacturing techniques are the key parameters that determine the performance of Solid Rocket Motors. Apart from design and manufacturing techniques, material selection plays a vital role in determining the performance of SRM [1]. SRMs consist of many components i.e. propellant grain, igniter, nozzle and casing or motor case. SRMs casings are also known as combustion chamber because all the combustion takes place inside the case. The case must withstand not only the structural loads but also the internal pressure due to the combustion process. Previously, the SRMs cases were made of metallic materials such as high strength steels and aluminum alloys. Now there is a shift towards the composite materials like glass fiber composites, carbon fiber composites and Kevlar. SRMs of varying sizes (diameter: 1.0 to 3.7 m, length: 20.0 to 55.0 m) have been used in different missions of space launches such as Ares (USA), Ariane (EU), Space Shuttles, PSLV (India) and GSLV.

In recent years, composite materials have gained increased usage in aerospace applications due to the significant weight reduction as compared to other engineering materials. At present, substantial research is being carried out on the fabrication of solid rocket motor cases from composite materials so that the advantage of the reduced weight of structural component to enhance rocket performance can be obtained [3]. Madhavi *et al.* [5] developed the methodology for layer sequence of the composite SRM and also calculated the necessary helical and hoop thicknesses for the shell to sustain the internal pressure. They carried out progressive damage failure analysis on geodesic domes and concluded that if hoop fibers are stacked on the outer surface of the helical fibers, the pressure sustainability is increased. Satish Kumar *et al.* [6] studied composite motor casings dome profiles and proposed an optimum design for a geodesic dome. They applied composite laminate theory along with other failure theories such as Tsai Wu and maximum stress theory and concluded that the hoop and circumferential layers fail before the longitudinal or axial layers. The layers having fiber orientation of 90° sustained more loads than that of 0° aligned fibers. Betti *et al.* [7] carried out the design analysis and experimental testing of composite SRM casings. They optimized the design parameters like dome geometry, winding angles, ply-sequence to minimize the composite case mass. Ravi Prakash *et al.* [8] presented a robust method to develop and test the laminate response against the load. In their study, the limitations and applications of various plate failure theories were compared and discussed. They also presented efficient FE model and least square error method for the accurate calculations of transverse shear stresses in composites and shear laminates. G. Avinash *et al.* [9] presented a study in which design analysis of composite SRM casing was compared with that of metallic SRMs casings. Maximum expected operating pressure and design pressure were compared with the ultimate strength of the materials to conclude the feasible and more suitable material. They showed that carbon fiber composite casings can sustain more pressure as compared to metallic casings. The result also showed that the performance factor of composite SRM is higher as compared to metallic SRM casings. They further recommended to substitute the metal case with carbon fiber composite case having a symmetric laminate code of  $[45_{18}/-45_{18}/90_{18}/0_{18}]_s$ .

The load carrying capacity of any SRM is directly related to its size. In order to increase the payload, the size of the SRM gets larger. Therefore it becomes difficult to manufacture it as a single segment. The segmented SRMs carry more payload due to its increased size.

<sup>1</sup>Samia Fida  
[Samiafida902@gmail.com](mailto:Samiafida902@gmail.com)

<sup>2</sup>Asif Israr

[Asif.Israr@yahoo.com](mailto:Asif.Israr@yahoo.com)

Department of Mechanical Engineering

Institute of space Technology, Islamabad, Pakistan.

Different segments of SRMs are joined together by field joint [4]. These joints must withstand the dynamic loads. In such case no compromise on the joint design, strength and its reliability can be made. After the accidental explosion of Space Shuttle Challenger in 1986, substantial research was carried out in structural and dynamic performance of field joints in segmented solid rocket motors (SRMs). Material and design modification of these joints increase the efficiency and reliability of the structures. Ghorouni *et al.* [10] presented the review on the redesigned field joint. In the present days, these redesigned field joints are used by the SRMs manufacturing industry. In the original field joint, the relative displacement between the tang and clevis resulted in the unseating of O ring that caused the historical accident of Space Shuttle Challenger. After that, a huge research was carried out to redesign the field joint that can resist the hot pressures due to the combustion of the gases. Based on this research, various factors that affect the field joint were varied to obtain the optimum parameter for redesigned field joint. In redesigned field joint Acrylo Butadiene Nitrile (ABN) was used as insulation material. Ghorouni *et al.* [10] further described the effects of shims, capture feature, and O rings in redesigned SRM joint. The shim, capture feature and O rings reduce the gap motion between the tang and clevis thus improving the reliability of the joint. They further described the effect of the size of the O rings on the joint strength along with the effect of filler. Both the factors improve the strength of the joint and prevent the leakage of the hot gases. Additional leak-check-port was added to examine the sealing efficiency of primary O-ring while leak-vent-port was used to remove the trapped air between the capture feature and tertiary O-ring. Micheal *et al.* [11] compared the axisymmetric analysis of both original field joint and redesigned field joint. In the original field joint there were only two O rings for the sealing purposes. In redesigned field joint a third O ring was added at the clevis inner face and the compression on all the three O rings was increased by setting the diameter value of 0.001 inch while the groove was machined to 0.005 inch. This configuration provided the improved pressurized sealing efficiency.

In redesigned field joints, various field joint parameters can be optimized. One of the parameter is the holding pin of tang and clevis. In SRM, field joint is held through pins. These metallic pins are assembled along the rows in holes of clevis and tang that grip and hold the joint. Increase in pin length along with holder width bands increases the reliability of the field joint. Pin arrangements around the field joint, pin diameter, pin material and total number of pins effects the joint strength. In this study all four parameters, described above, are to be evaluated against joint reliability to obtain the optimum factors that yield the most efficient joint. After the selection of optimum joint parameters, the progressive damage analysis is carried out to analyze the behavior of composite solid rocket motor segment joint against the proposed operating conditions. This is done to find out the critical failure mechanism of composite SRM.

## II. DESIGN AND MODELING OF SEGMENT JOINT

Modeling of the segment joint is carried out in *CAD* while analysis have been performed in *Ansys 16.1*.

### i. Numerical Study for Critical Number of Pins

The critical number of pins is calculated on the basis of specifications described in *Table 1*. All the calculations are as per the standard pressure vessel design codes. The formulas used are for the plates; however, it is generally assumed that these are also applicable for the cylindrical shaped vessel. In segmented joint, pressure, tension and shear forces cause failure in pin/bolts/bearing, plate and plate bearing respectively. All of the three above mentioned forces act in solid rocket motors. Hence hoop stress and axial stress are the two components that arise due to internal pressure. At the segment section of the solid rocket motor, the load is sustained by the number of pins as shown in *Fig.1*.

TABLE 1  
MOTOR SPECIFICATIONS

Motor Diameter (external)	550mm
Casing thickness	7mm
Design pressure	80 bar
FoS (Factor of Safety)	1.2

Using the equilibrium law

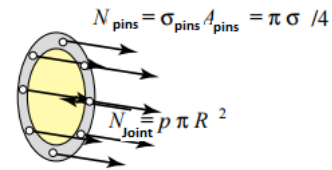


Fig.1. Load sustained by the pins [13]

$$N_{pins} = N_{joint} \quad (1)$$

$$n \sigma_{pins} \frac{\pi}{4} d_{pins}^2 = \sigma_{joint} w_{joint} \tau_{joint} \quad (2)$$

The stress sustained by the joint is the hoop stress so

$$\sigma_{joint} = \sigma_{hoop} \quad (3)$$

Where

$$\sigma_{hoop} = \frac{Pr}{\tau} \quad (4)$$

Substituting the value of Eqn 4 in Eqn 2, we get relation of number of pins

$$n = \left[ \frac{\Pr(w_{joint} \tau_{joint})}{t} \left( \frac{1}{0.78 \sigma_{pins}} \right) \right] \frac{1}{d_{pins}^2} \quad (5)$$

Substituting the values of geometrical parameters of the Joint, we get

$$n = 2389.7 \left( \frac{1}{d^2} \right) \quad (6)$$

Eqn 6 gives the relationship between the number of pins and the diameter of the pins. Starting from the diameter of 4mm (as commercially available diameters for aerospace pins range from 4mm to 20 mm), we obtain number of pins, tabulated in Table 2.

TABLE 2  
DIAMETER VS NUMBER OF PINS

Sr #	Diameter (mm)	Number of pins
1.	4	146
2.	6	65
3.	8	37
4.	10	24
5.	12	17
6.	14	12
7.	16	10

TABLE 3  
PIN MATERIALS AND PROPERTIES

Sr No.	Material	Yeild Strength (ksi)	Modulus of Elasticity (1000 ksi)	Density (lb/m <sup>3</sup> )
1.	HY-130/150	150	29.5	0.285
2.	D6AC	240	29	0.283
3.	Ti-6Al-4V	150	16	0.167
4.	Aluminum 7076	68	10.3	0.10

#### i. Pin Material

Different pin materials are used as shown in Table 3 to find out the prime material for pins.

#### ii. Pin configuration

Two different pin configurations i.e. linear and zig zag are analyzed and compared to evaluate the effect of stress distribution in both cases. The change in pin configuration also affects the joint strength. Thus the comparison gives the most effective configuration with minimum deformation and less stress.

#### iii. Modeling of Joint using CAD and ANSYS

The geometry is designed using CAD tool and analysis is performed on sliced part of the geometry because of symmetry as shown in Fig.2 (a) and (b). The basic parts of the designed joint include the composite case, metallic joint section, O-rings sealing and pins. All the material properties are provided in Table 4(b) while composite properties are shown in Table 4

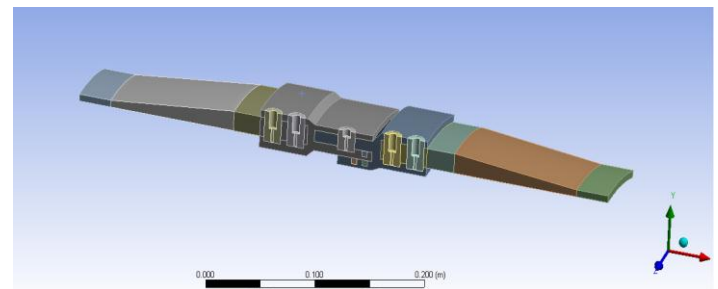


Fig.2(a). Complete Joint geometry

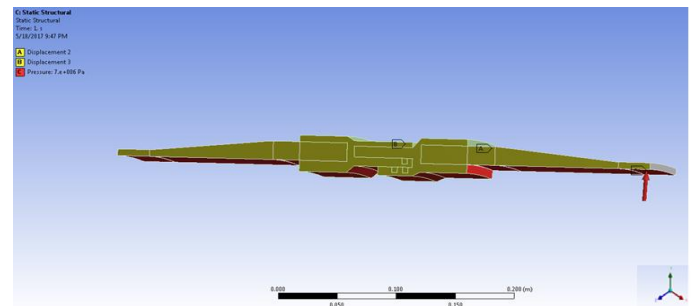


Fig.2(b). Boundary conditions applied to the joint geometry

(c). Composite casing is modeled using ACP Pre. Hex Dominant method is used for the meshing of metallic joint which reduces the number of elements. In Hex Dominant Method majority of the cells are hex type, while some tetrahedral and pyramid cells are created for better conformance with the geometry. As pins and O-rings are sweepable bodies so sweep mesh is carried out. Table 4(a) provides the summary of mesh methods used. Complete mesh assembly is shown in Fig.3.

TABLE 2  
MAX STRESS AND DEFORMATION FOR VARYING NUMBER OF PINS

Sr. No.	Diameters (mm)	No of Pins	Stress(MPa)	Deformation(m)
1	16	10	1047	0.0088
2	14	12	968	0.0093
3	12	17	924	0.0090
4	10	24	978	0.0032
5	8	37	978	0.00915
6	6	64	1021	0.00904
7	4	146	1103	0.00906

The mesh refinement is carried out through body, edge and face sizing for better solution.

TABLE 4 (b)  
SUMMARY OF MATERIAL MODELS

Parts	Material Models		Element Type
	Material	Properties	
Joint Section	D6AC	Linear-elastic-Isotropic	Hex type
Pins	HY-130/150 D6AC Ti-6Al-4V Aluminum 7076	Linear-elastic-Isotropic	Quad/Tri
O-rings	Rubber	Hyper Elastic	Quad/Tri
Composite Casings.	Carbon Fiber Reinforced Composite	Composite Properties Table 4(c)	Shell Element

TABLE 4(c)  
LAYER SEQUENCE WITH THICKNESS

Layer #	Orientation	Thickness(mm)
1	34	0.75
2	-34	0.75
3	45	0
4	-45	0
5	90	3
6	-45	0
7	45	0
8	-34	0.75
9	34	0.75
Total Thickness		6

III. RESULTS AND DISSCUSIONS

After generating the mesh of the joint assembly, the boundary conditions are applied. The body is constrained in x and z direction and internal pressure of 7 MPa is applied. Because of this pressure the SRM case experiences expansion in the axial and hoop direction as shown in Fig 2(b). In the next phase various analysis are performed which are discussed in detail below:

i). Structural Analysis

The structural analysis is performed for seven different diameters, four different pin materials and two different configurations. In case of varying diameters of 4mm to 16mm,

TABLE 3(a)  
SUMMARY OF MESH METHODS

Parts	Mesh Properties			
	Mesh Method	Element Type	Refinement	Mesh Independence
Joint Section	Hex Dominant method.	Hex type	Body sizing (2x10 <sup>-3</sup> )	Checked
Pins	Sweep method	Quad/Tri	Edge Sizing (19 divisions)	
O-rings	Sweep method	Quad/Tri	Face Sizing (1x10 <sup>-3</sup> )	
Composite Casings.	ACP Pre	Shell Element		

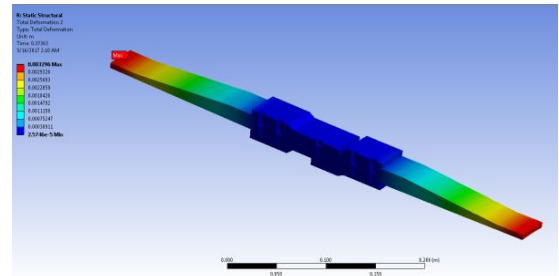


Fig.4. Maximum deformation for pin diameter of 12mm

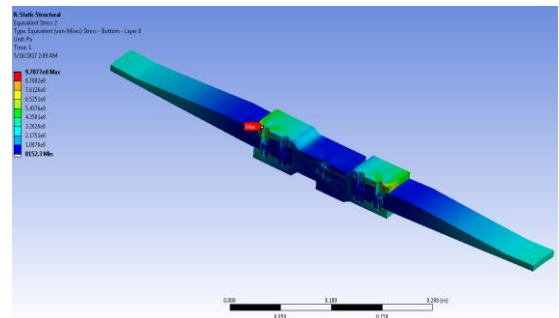


Fig.5. Maximum von misses stress for pin of 12mm the stress and deformation obtained are given in Table 5.

The analysis for diameter of 12mm is shown in Fig. 4 and 5. The deformation plots show that, at the given operating conditions, there is no deformation produced in metallic joint sections as shown in Fig.4. It can be seen that deformation is produced at the ends of composite casings. Since the composite thickness is less at the ends of the casings and joint rotation causes bending forces that produce maximum deflection at the

ends. The joint is stiff as compared to composite casing. Thus the joint resists the internal pressure and as a result maximum deflection is produced at the casing ends. This deformation can further be reduced by optimizing the ply sequence and thickness at the casing ends. *Table 5* show the variation of Von misses stress with varying pin diameter. The maximum deformation appears at pin locality as shown in *Fig.5*. It can be seen that as the diameter decreases the maximum stress decreases initially, giving prime value at 12mm and increases again. The decrease in diameter reduces the stress concentration due to large holes thus reducing the max stress. Further reduction in diameter causes the area loss that increases

the net stress concentration factor and increases the max stress again. The similar trend with varying number of bolts was observed by Harts Smith for bolted composite laminate plates [12]. Initially, by increasing the bolt diameter the joint strength was improved giving a prime value. With further increase in the diameter, the joint strength decreased again *Table 6* shows the variation of maximum stress and maximum deformation with yield strength and modulus of elasticity of pin material. As the stiffness of the pin material increases, the maximum stress increases due to increase in bearing strength of the pin material. This causes more deformation of the composite material at the joint composite interface. Thus the least stiff material among the candidate materials has been selected for analysis purpose as it gives minimum deformation at composite-joint interface.

TABLE 6  
EFFECT OF VARYING MATERIALS ON JOINT STRENGTH

Sr No.	Material	Yield strength (ksi)	Elastic Modulus (1000 ksi)	Max Stress (Von Misses) (ksi)	Max Deformation (m)
1.	HY-130/150	150	29.5	168	0.00882
2.	D6AC	240	29	166	0.00882
3.	Ti-6Al-4V	150	16	138	0.00882
4.	Aluminum 7076	68	10.3	135	0.00882

Two varying pin configurations are compared and analyzed i.e. linear and zig zag. The stress distribution varies across both the pin configurations. This distribution is more uniform in case of linear configuration as compared to zig zag as shown in *Fig.6*. The linear configuration of the pins provides a better defense hole system that reduces the stress concentration due to in line holes. Linear arrangement of the pin also minimizes the peel stress at the joint ends thus making the joint design more reliable and efficient.

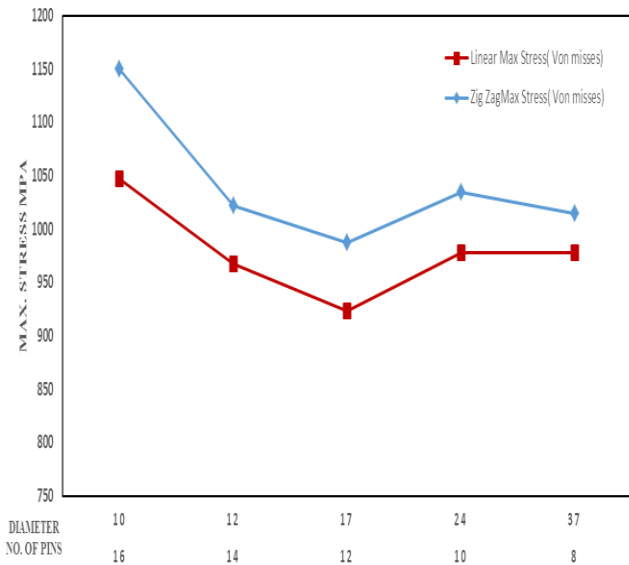


Fig.6. Effect of varying configurations on maximum stress

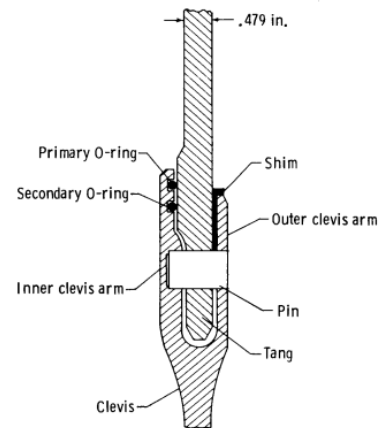


Fig.7. Cross section of Tang-clevis Joint [12]

TABLE 7  
COMPARISON OF THE STRESS ANALYSIS OF WITH THE REFERENCE GEOMETRY

Type	Reference geometry for the reference operating conditions( reproduced)	Reference geometry for the proposed operating condition	The proposed geometry with reference operating conditions
Units	(MPa)	(MPa)	(MPa)
Hoop Stress at pin locality	1716	1668	924
Hoop Stress at shell	661	521	520
Axial Stress at pin locality	1068	821	468
Axial Stress in shell	524	504	480

[12]. In the referred research work the structural analysis of tang clevis joint was performed that creates ground for the construction of metallic segmented solid rocket motors. The cross section of the geometry is shown in Fig.7. In FE analysis, the internal pressure of 6.92 MPa was applied and resulting axial and hoop stresses were measured. For experimental study, the hydrostatic pressure of 6.92 MPa was applied and resulting strain was measured using strain gauges at and near the joint areas. FE and experimental analysis for the given operating conditions showed that the hoop stress at the joint area close to the pin was maximum, whereas the shell area shows low value of hoop stress. Same trend is observed for the axial stresses. The hoop and axial stresses for the reference geometry are given in Table 7.

The maximum stress appears near the pin hole due to stress concentration and the hoop stress increases as the joint faces the moments. Clevis moves outward however pin resists this movement. As a result the stress concentration appears in pin locality. The comparison presented in Fig.8 shows that the proposed geometry exhibits better resistance to hoop and axial stresses as compared to the reference geometry. Thus, the use of proposed geometry gives better factor of safety with more pay load.

ii). *Algorithm for Progressive Damage Analysis*  
Carbon/ Glass Fiber composites have outstanding strength to weight ratio that makes these composites an excellent candidate for structural materials in aerospace industry.

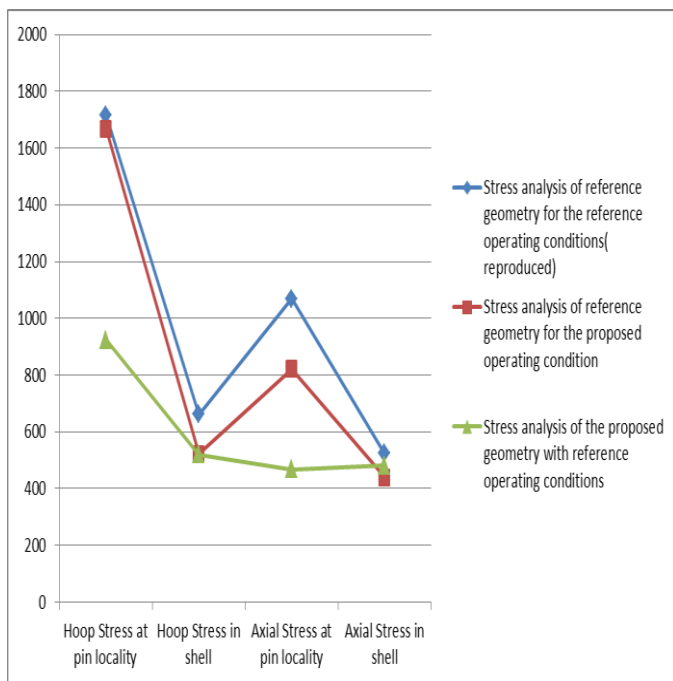


Fig.8. Comparison of the Reference Geometry with Proposed Geometry

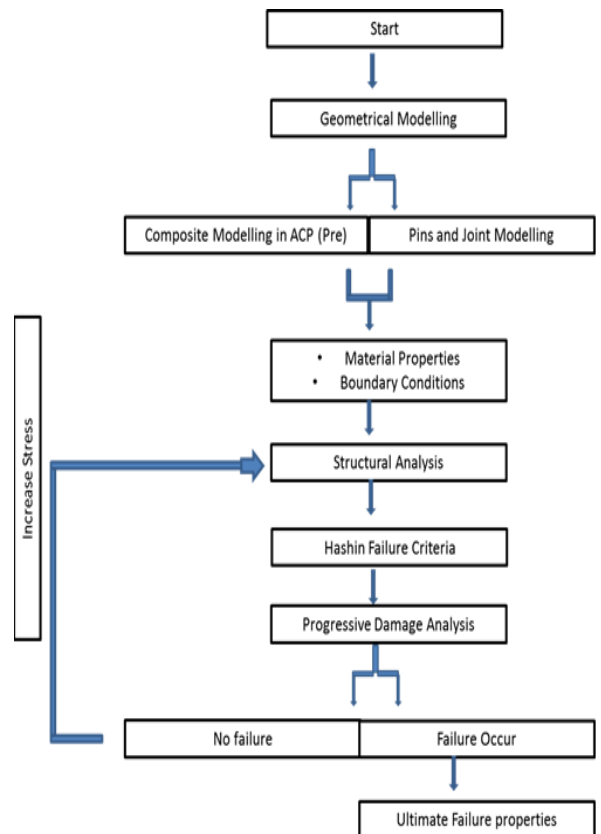


Fig.9. Algorithm for Progressive Damage Analysis

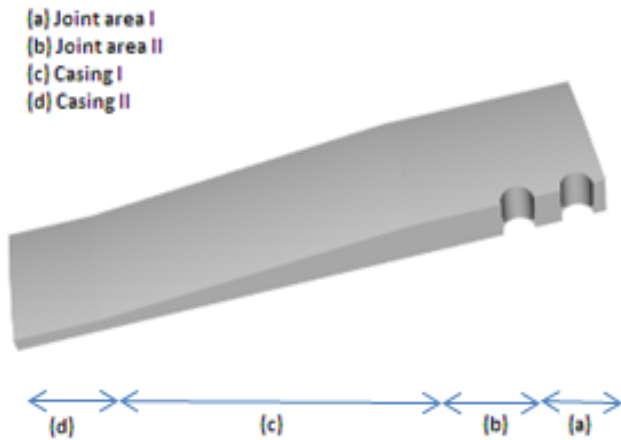


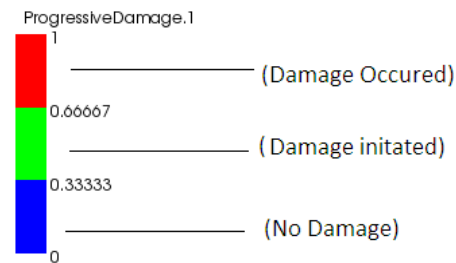
Figure 10: Composite casing showing tapered thickness

The drawback of fiber composite lies in their non-isotropic behavior. The fiber composites have better mechanical properties in planer direction as compared to through thickness direction. This makes the composite structures very vulnerable to impact loads with low velocity. A low velocity impact causes invisible damage in terms of matrix cracking that is followed by the delamination of layers. As a result the fiber breakage occurs that completely collapses the structure. Thus progressive damage analysis is the most promising technique to evaluate the actual behavior of composite materials. To evaluate the mechanical performance of composite structure the damage mechanism and its progression is important. An algorithm is defined for the progressive damage analysis as shown in *Fig.9*. The optimum number of pins and optimum material properties are selected based on the results of structural analysis to perform progressive damage analysis. This algorithm uses the Hashin criterion to calculate the stiffness of the structure. As one ply fails, the stiffness of the structure is reduced. That reduced stiffness is calculated to sustain the applied pressure until all the plies fail and total stiffness of the structure becomes zero. In this study, the progressive damage accumulation is analyzed for the composite part of the casing for the operating pressures of 1 to 7 MPa. The material of the pin that is Al 7076 and pin diameter of 12mm is selected as both parameters give the minimum stress and minimum deformation. The progressive damage analysis for fiber failure, matrix failure and damage status is evaluated. The fiber tensile failure, fiber compressive failure and matrix compressive failure are known as fatal failures. The matrix tensile failure is known as non-fatal failure. The fiber tensile, fiber compressive, matrix tensile and matrix compressive failure for 1 to 7 MPa are compared in *Fig.10*.

The analysis shows that for different thickness of the composite, the matrix and fiber behavior towards failure is different. The composite casings are tapered i.e. the thickness varies from joint section to the casing ends. At the joint section the thickness is maximum that is 17mm and it reduces gradually towards the end, which is 6mm as shown in *Fig.11*.

It can be seen from the analysis that the fiber compressive failure does not contribute towards damage as there is no applied compressive stress on the fibers. Damage due to matrix tensile failure is more dominant at 2 MPa. The reason is that the tensile component causes the fiber pull out due to more deformation in matrix as compared to stiff fibers. The matrix damage occurs due to both matrix compressive as well as matrix tensile failure. Matrix tensile failure is more dominant in the casing sections I and II as the thickness of the ply is very high. As the number of plies decreases the ply thickness increases which increase the inter-laminar shear strength thus matrix tensile failure occurs. As the stress increases, decohesion between the fiber and matrix causes compressive failure of the matrix. Furthermore, the fewer layers at the ends are not able to withstand the hoop stress generated by the internal pressure.

The total damage results show that the damage due to matrix tensile failure is more critical towards cumulative damage as compared to the fiber failure as shown in *Fig.10*. The damage starts at 2 MPa and increases with stresses. At the joint area the damage is very low and is high towards the ends. The progressive damage for each successive layer at the pin bearing areas of the joint is shown in *Fig. 12*. The damage is more dominant in outer plies as compared to the inner. The reason of this failure is that the internal pressure creates a state of bi-axial stress in the composite lamina in which the maximum stress occurs at  $90^\circ$  lamina that progresses towards the upward laminates because of hoop stress. In angle ply the transverse ply cracking occurs and initiates at low level stress due to stress concentration at any fiber matrix defect. Apart from this bi-axial stress, upper plies undergo bending due to expansion created by the internal pressure. This involves both matrix cracking and fiber-matrix de-bonding. As the stress increases, the saturation point is achieved that is the propagation of cracks. This produces the characteristic damage state as shown in *Fig.12*



Pressure (bar)	Fiber Compressive	Fiber Tensile	Matrix Compressive	Matrix Tensile	Damage Status
10					
20					
30					
40					
50					
60					
70					

Fig.11. Damage accumulation from 10-70 bar for different failure modes.

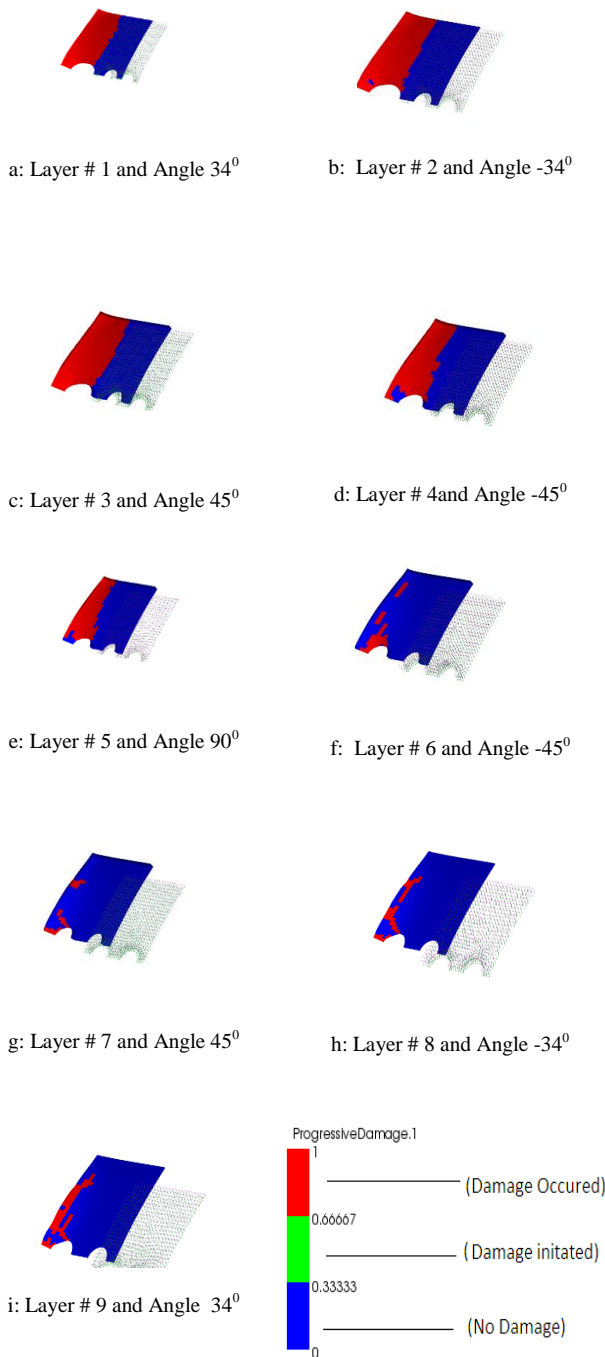


Fig.12. Progressive damage analysis in different layers

#### IV. CONCLUSION

Internal pressure of solid rocket motor develops hoop stress that expands the solid rocket motor case. For the proposed joint design, structural and progressive damage analysis is performed to evaluate the behavior of composite SRM joint. From the results following outcomes are achieved:

- i. For the given operating conditions, pin material Al 7076 gives the optimum properties with minimum stress due to low bearing strength of the alloy.
- ii. The pin diameter of 12mm gives the optimum structural properties with minimum stress and minimum deformation as a result of better conformance between tang and clevis.
- iii. Progressive damage analysis shows that the matrix tensile failure is more critical towards cumulative damage as compared to fiber failure.
- iv. The matrix failure starts from lower plies due to bi-axial stress state in the composite lamina in which the maximum damage occurs at 90° lamina that progresses towards the upward laminates.
- v. For the given operating conditions the proposed pin material, number of plies and ply sequence of the joint show negligible deformation thus the joint sustains the operating pressure up to 4 MPa.
- vi. Cumulative damage at the shell (case) is more as compared to the joint as thickness of the plies at composite shell is high. This damage can be minimized by decreasing the thickness of the ply thus incorporating more angle plies to achieve the optimum thickness for the composite shell.

#### V. REFERENCES

- [1] D. K. Cowles, "Design of a Rocket Motor Casing," Rensselaer Polytechnic Institute Hartford, May, 2012.
- [2] I. B. Zandbergen, "Some Typical Solid Rocket Propellant," Decemeber, 2013.
- [3] A. L. Highsmith, "Post Impact Behaviour of Composite Solid Rocket Motor Cases" ,1992.
- [4] N. Knight, R. Gillian and M. Nemeth, "Non Linear Shell Analysis of the Space Shuttle Solid Rocket Boosters," *Springer Series in Computational*, pp. 305-326, 1990.
- [5] M. Madhavi and K. Rao, "Design and Analysis of Filament Wound Composite Pressure Vessel with Integrated End Domes," *Defense Science Journal*, pp. 73-81, 2009.
- [6] D. Kumar and S. Nayana, "Design and Structural Analysis of Solid Rocket Motor Casing Hardware.," *International Journal of Engineering Research and Technology*, vol. 5, no. 2, 2016.
- [7] F. Betti, P. Perugini and A. Mataloni, "Design and Development of Vega Solid Rocket Motor Composite Cases," in *43rd ASME*, 1989.
- [8] R. Khandelwal Prakash, A. Chakrabart and B. Pradeep, "An Efficinet FE Model and Least Square Error Method For Accurate Calculation of Transverse Shear Stresses in Composite and Sandwich Laminates," *CompositesPart B Engineering*, pp. 1695-1704, 2012.
- [9] G. Avinash, D. S. R. Krishna and N. K. Shrivastava, "Design and Analysis of Composite Rocket Motor Casing," *International Journal of Emerging Technology and Advanced Engineering*, vol. 4, no. 6, pp. 231-236, 2014.
- [10] Gharouni and S. Mohammad, "Space Shuttle Solid Rocket Motor Field Joint; Review Paper," *Association of Metallurgical Engineers of Serbia*, vol. 20, no. 3, pp. 155-163, 2014.
- [11] Michael, P. Nemeth, S. Melvin and Anderson, "Axisymmetric Shell Analysis of Space Shuttle Solid Rocket Booster Field Joint," *Journal of Spacecraft and Rockets*, vol. 27, no. 1, pp. 85-92, 1990.
- [12] L. H. Smith, "Bolted Joint in CFRP composites". United States Patent 13172, 01 06 1976.
- [13] R. C. Hibbler, "Thin Pressure Vessel," in *Mechanics of Materials* , 2010.